Journal of Alloys and Compounds 935 (2023) 167912

Contents lists available at ScienceDirect

Journal of Alloys and Compounds

journal homepage: www.elsevier.com/locate/jalcom

Linear and nonlinear optical properties of trigonal borate crystals $K_7MIn_{2-x}Yb_x(B_5O_{10})_3$ (M = Ca, Sr, Ba; x = 0…2) with isolated B_5O_{10} units

A.Y. Jamous [a,*], V.A. Svetlichnyi [a], A.B. Kuznetsov [b], K.A. Kokh [b,c,d], N.G. Kononova [b], I.N. Lapin [a], A. Bolatov [e], Y.A. Zholdas [e], A.E. Kokh [b]

[a] Tomsk State University, Tomsk 634050, Russia
[b] Crystal Growth Lab, Sobolev Institute of Geology and Mineralogy SB RAS, Novosibirsk 630090, Russia
[c] Geology-geophysics department, Novosibirsk State University, Novosibirsk 630090, Russia
[d] Kemerovo State University, Kemerovo 650000, Russia
[e] Center of Physical-Chemical Methods of Research and Analysis, Al-Farabi Kazakh National University, Almaty 050040, Kazakhstan

ARTICLE INFO

Article history:
Received 3 October 2022
Received in revised form 1 November 2022
Accepted 3 November 2022
Available online 9 November 2022

Keywords:
Borate
Crystal structure
Raman
Photoluminescence
Second harmonic generation (SHG)
Self-frequency doubling (SFD)

ABSTRACT

Noncentrosymmetric borates $K_7MIn_{2-x}Yb_x(B_5O_{10})_3$ (M = Ca, Sr, Ba; x = 0…2) were synthesized by the solid state reaction and the crystals were successfully grown by the top seeded solution growth method using the K_2O-B_2O_3-MF_2 flux. According to Rietveld refinement, the crystal structure belongs to the noncentrosymmetric *R*32 space group. Also, the octahedrally coordinated In atoms are located at wide ranges ~8 Å which may be promising for phosphor and laser applications. Samples with ytterbium show a characteristic emission band in the range of 950–1050 nm related to the $^2F_{5/2} \rightarrow {}^2F_{7/2}$ transition of Yb^{3+} ions that is commonly used for laser generation. IR, Raman and absorption spectra were obtained for the samples as well. The short cut edge of UV absorption, SHG intensity comparable with KDP and low concentration quenching of luminescence suggest that the $K_7MIn_{2-x}Yb_x(B_5O_{10})_3$ borates are promising self-frequency doubling materials.

1. Introduction

Today a large amount of research is aimed at the development of materials used as new generation environmentally friendly light sources and phosphors, as well as nonlinear optical materials and self-frequency doubling (SFD) crystals [1–6]. One of the promising classes of such materials are borates, which have high chemical stability, thermal and radiation resistance, a wide area of transparency and a high threshold of laser destruction [7–10]. In addition, borates have a wide variety of chemical composition and crystal structure, which correlates with the ability of the boron atom to form various anionic ($[BO_3]^{3-}$, $[BO_4]^{5-}$) and polyanionic groups ($[B_3O_6]^{3-}$, $[B_2O_7]^{8-}$, $[B_5O_{10}]^{5-}$ and etc.) [11]. The combination of laser generation with a wide area of transparency in the ultraviolet range and a high threshold of laser destruction opens the way to active nonlinear crystals for borates of rare earth elements. That borates can be simultaneously perform the functions of a coherent radiation source and a nonlinear optical frequency converter, for example, YCOB ($Ca_4YO(BO_3)_3$) [12], YAB ($YAl_3(BO_3)_4$) [13].

In works [14,15] authors have reported two noncentrosymmetric borates $K_3YB_6O_{12}$ and $K_6Li_3Sc_2B_{15}O_{30}$ crystallizing in noncentrosymmetric space group *R*32. Possible isomorphous substitutions of cation part in these compounds are noted providing materials with new properties. Also, a wide transparency region from 190 to 3000 nm, the second harmonic generation (SHG) efficiency higher than for KH_2PO_4 (KDP) are characteristic for $K_3YB_6O_{12}$ and $K_6Li_3Sc_2B_{15}O_{30}$ which allow them to be used as nonlinear optical or SFD materials for doped f- d elements. In our papers [16,17] noncentrosymmetric borate $K_7CaY_2(B_5O_{10})_3$ has been obtained for the first time by heterovalent and isovalent substitutions in $K_6Li_3Sc_2B_{15}O_{30}$. Also series of compounds $K_7M^{II}RE_2(B_5O_{10})_3$ (M^{II} = Ca, Sr, Ba, K/$RE_{0.5}$; RE = Y, Lu, Gd) are shown in paper [18].

However, any information in the literatures on the synthesis and study of the physico-chemical properties of indium pentoborates has not found. While the location of In in the third group together with Sc, Y, La and lanthanides suggests similar properties and the possibility of isomorphic substitution [19–23]. At the same time, use of acentric luminescent matrices containing Yb^{3+} is attractive as active media for SFD lasers [24–26].

* Corresponding author.
E-mail address: ammarjamous2@gmail.com (A.Y. Jamous).

https://doi.org/10.1016/j.jallcom.2022.167912
0925-8388/

In this work, the bulk crystal of noncentrosymmetric borate $K_7MIn_2(B_5O_{10})_3$ and $K_7MYb_2(B_5O_{10})_3$ (M = Ca, Sr, Ba) has been obtained by top seeded solution growth method using K_2O- B_2O_3-MF_2 flux. The optical properties of $K_7MIn_{2-x}Yb_x(B_5O_{10})_3$ such as SHG, IR, Raman and absorption spectra, were tested.

2. Experimental procedures

2.1. Synthesis and crystal growth

A polycrystalline samples of $K_7MIn_{2-x}Yb_x(B_5O_{10})_3$ (M = Ca, Sr, Ba; x = 0…2) were prepared by the method of two stage solid state synthesis in a Pt crucible. The stoichiometric mixtures of pure raw K_2CO_3, $CaCO_3$/SrCO3/$BaCO_3$, H_3BO_3 and In_2O_3/Yb_2O_3 reactants were heated at 650 °C for 5 h to decompose K_2CO_3, $CaCO_3$/SrCO3/$BaCO_3$, and H_3BO_3. At the second stage, the mixtures were grinded in agate mortar and heated again at 800 °C for 12 h until the powder X-ray method showed no peaks of initial compounds. After that, the samples $K_7MYb_xIn_{2-x}(B_5O_{10})_3$ (step 0.2) were prepared and heated to 800 °C for 12 h.

2.2. X-ray diffraction and elemental analysis

The syntheses samples of $K_7MIn_2(B_5O_{10})_3$ and $K_7MYb_2(B_5O_{10})_3$ (M = Ca, Sr, Ba) were studied with XRD. Powder X-ray diffraction patterns of powdered samples were obtained with the XRD 7000 (Shimadzu, Japan) diffractometer in Bragg-Brentano geometry using CuKα radiation at room temperature (Fig. 2). The crystal structure of obtained samples was refined by Rietveld method which was performed using GSAS-II. The crystal structure of $K_7CaIn_2(B_5O_{10})_3$, $K_7CaYb_2(B_5O_{10})_3$, $K_7SrIn_2(B_5O_{10})_3$, $K_7SrYb_2(B_5O_{10})_3$, $K_7BaIn_2(B_5O_{10})_3$ and $K_7aYb_2(B_5O_{10})_3$ was used as starting model for refinements with practical replacement in R^{3+} positions. All ions were refined with isotropical thermal parameters; moreover all O^{2-} and B^{3+} ions were refined with one thermal parameter in order to reduce the number of parameters. Final refinements were stable and gave low *R*-factors. Summary data about the XRD, data-collection parameters, and the structure refinement of $K_7MIn_2(B_5O_{10})_3$, $K_7MYb_2(B_5O_{10})_3$ syntheses at 800 °C are listed in Tables S1, S2 and exploded charts in Fig. 1S, respectively. Final atomic coordinates, equivalent isotropic displacement parameters are reported in Tables S3-S8.

The chemical composition of obtained crystals was measured by X-ray fluorescent analysis using XRF 1800, Shimadzu. The results of analyses are in a good agreement with the formulae obtained after crystal structure refinement.

2.3. Thermal properties

The thermal properties of powdered samples of $K_7CaIn_2(B_5O_{10})_3$, $K_7CaYb_2(B_5O_{10})_3$, $K_7SrIn_2(B_5O_{10})_3$, $K_7SrYb_2(B_5O_{10})_3$, $K_7BaIn_2(B_5O_{10})_3$ and $K_7BaYb_2(B_5O_{10})_3$ syntheses at 800 °C were investigated by the differential scanning calorimetry (DSC) using scanning thermal analyzer 449 F5 Jupiter (Netzsch, Germany). A 50 mg of powdered samples was placed in a platinum crucible and heated with argon as a carrier gas from room temperature to 1100 °C at the rate of 20 K.min^{-1}. An empty Pt crucible was used as a standard.

2.4. Fluorescence properties and SHG

The luminescence spectra of powdered $K_7MIn_{2-x}Yb_x(B_5O_{10})_3$ (M = Ca, Sr, Ba; x = 0…2) were collected using InVia Raman microscope under the excitation of 785 nm CW diode laser in the range of 800–1100 nm.

The SHG efficiencies of the studied crystals have been evaluated using the conventional Kurtz-Perry powder technique [27]. Samples were illuminated by nanosecond pulses of the Q-switched Nd:YAG laser (LS-2132UTF, LOTIS TII, Belarus) at the fundamental wavelength λ = 1064 nm with a pulse width of τ = 7 ns and pump power densities in the range of 5–70 MW/cm^2. The SHG intensity was measured by a DET100A (Thorlabs, USA) Si diode located behind a series of filters removing the fundamental beam. Powders were graded by use of standard sieves to the desired range of particle sizes: 20–40, 40–56, 56–64, 64–80, 80–100, 100–125, 125–140 and 140–200 µm. KDP samples with the same size ranges were used as references.

The effective nonlinearity coefficient was calculated for particle sizes larger than 100 µm using the following formula [28]:

$$d_{eff} = \sqrt{I_{SHG}/I_{SHG}(KDP)}.\ d_{eff}(KDP)$$

The value of d_{eff} (KDP) is equal to 0,27 pm/V (d_{36} = 0,39 pm/V) when Kleinman symmetry holds [29]. The reliability of the obtained results is ensured by the fact that KDP and our crystals, being members of $\bar{4}2m$ and 32-point groups respectively, have a similar formula of effective nonlinearity coefficients [30].

3. Results and discussion

3.1. X-ray diffraction, elemental analysis and structure

According to powder X-ray diffraction of samples $K_7CaIn_{2-x}Yb_x(B_5O_{10})_3$, $K_7SrIn_{2-x}Yb_x(B_5O_{10})_3$ and $K_7BaIn_{2-x}Yb_x(B_5O_{10})_3$ annealed at 800 °C (Fig. 2S) they all are isotypical and crystalized in *R*32 space group with unit cell parameters shown in Table 9 S. The

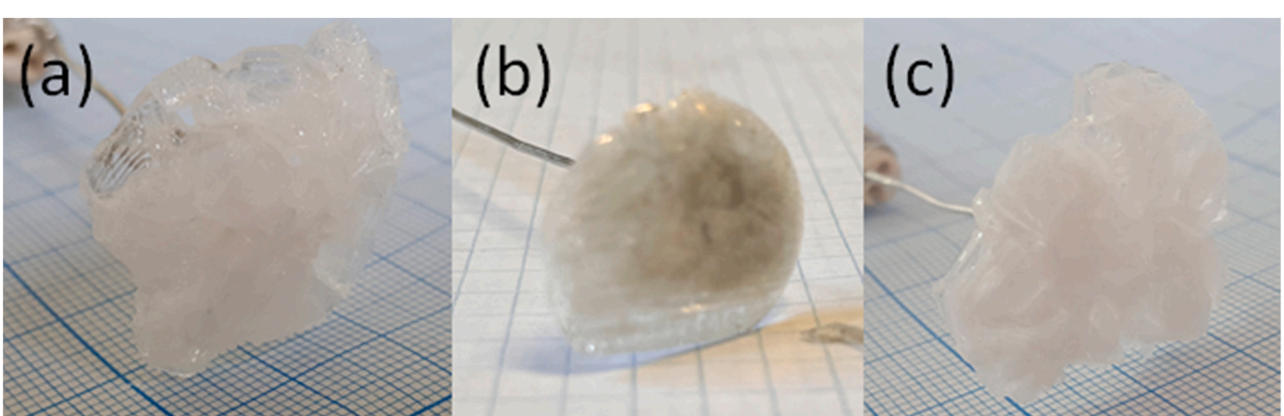

Fig. 1. Crystals of: a) $K_7CaIn_2(B_5O_{10})_3$, b) $K_7SrIn_2(B_5O_{10})_3$, and c) $K_7BaIn_2(B_5O_{10})_3$.

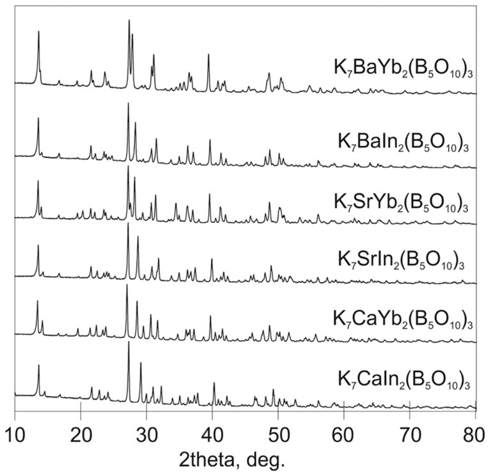

Fig. 2. XRD powders of $K_7MR_2(B_5O_{10})_3$ (M = Ca, Sr, Ba; R = In, Yb).

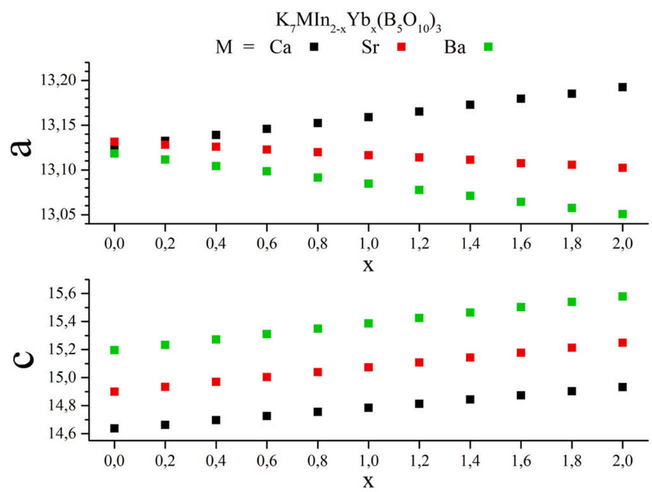

Fig. 3. Unit cell parameters of $K_7MIn_{2-x}Yb_x(B_5O_{10})_3$ (M = Ca, Sr, Ba) solid solutions.

dependencies of the unit cell parameters of solid solutions are showed in Fig. 3. According to these data, it can be concluded that a significant increase in the unit cell parameters occurs in the *c* direction. Thus, an increase in the cation radius M and R leads to stretching of the structure along *c*.

According to Rietveld refinement, $K_7MR_2(B_5O_{10})_3$ (M = Ca, Sr, Ba; R = In, Yb) crystalizes in the trigonal crystal system with a space group *R*32. The structure framework is composed of R-M-R-K chains located on the 3rd order screw axis. R and M atoms occupy distorted octahedron positions and K1 atoms are surrounded by twelve oxygen atoms [6 + 6]. Three B_5O_{10} groups form the "propeller blades" around K1 polyhedron and bond R-M-R chains together. The shortest distance between R atoms is determined by the M cation. According to [31] The M cations Ca, Sr and Ba for octahedral coordination have the following ionic radii 1, 1.18 and 1.35 Å, respectively. Thus, changing the cation at position M allows you to change the distance between R cations within 6.71 Å, 6.72 Å and 7.0 Å for Ca, Sr and Ba, respectively (Fig. 4).

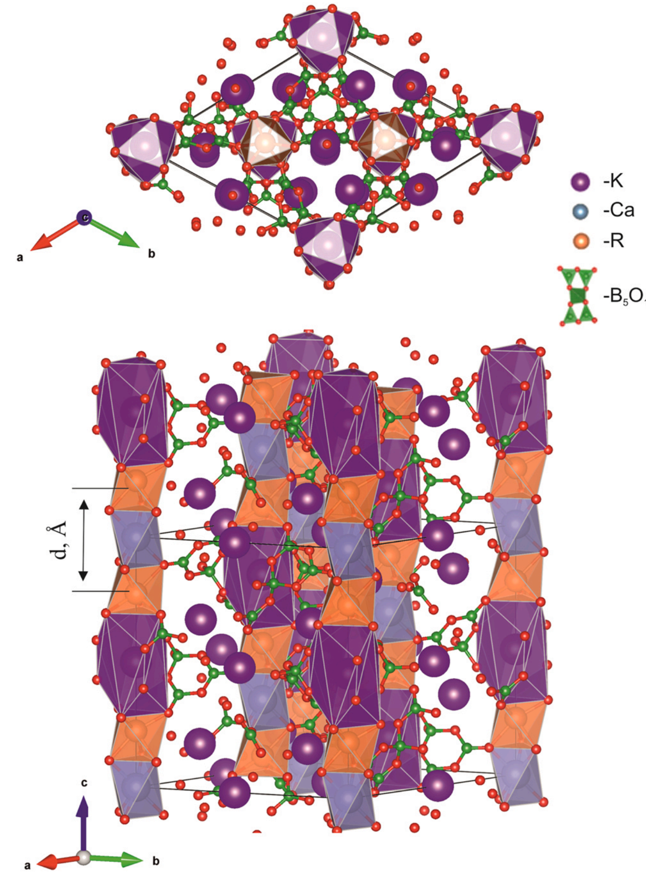

Fig. 4. Structure of $K_7MR_2(B_5O_{10})_3$ (M = Ca, Sr, Ba; R = In, Yb).

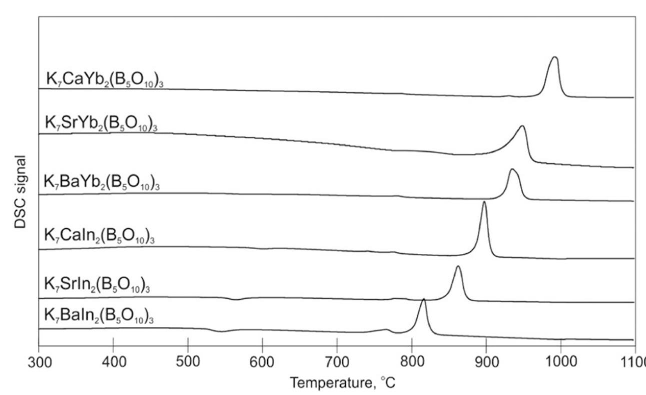

Fig. 5. DSC curve of $K_7MR_2(B_5O_{10})_3$ (M = Ca, Sr, Ba; R = In, Yb).

3.2. Thermal properties

As shown in Fig. 5, the all DSC curve of $K_7MR_2(B_5O_{10})_3$ (M = Ca, Sr, Ba; R = In, Yb) has one endothermic peak of melting on the heating curve at 923 °C (Ba), 952 °C (Sr) and 973 °C (Ca) for Yb series and 801 °C (Ba), 848 °C (Sr) and 885 °C (Ca) for In series. The present data evidence incongruent melting at least for $K_7CaY_2(B_5O_{10})_3$ since the sample after DSC analysis shows YBO_3 peaks on the X-ray diffraction pattern [16]. However, no peaks on XRD pattern for $K_7MR_2(B_5O_{10})_3$ (M = Ca, Sr, Ba; R = In, Yb) crystals were observed. It is likely to associated with glass transitions of this compounds, which are incongruent melting like compound with Y.

3.3. Optical properties

3.3.1. Luminescence

The normalized luminescence spectra of the samples of $K_7MYb_2(B_5O_{10})_3$ are plotted in Fig. 6(a), These materials exhibit

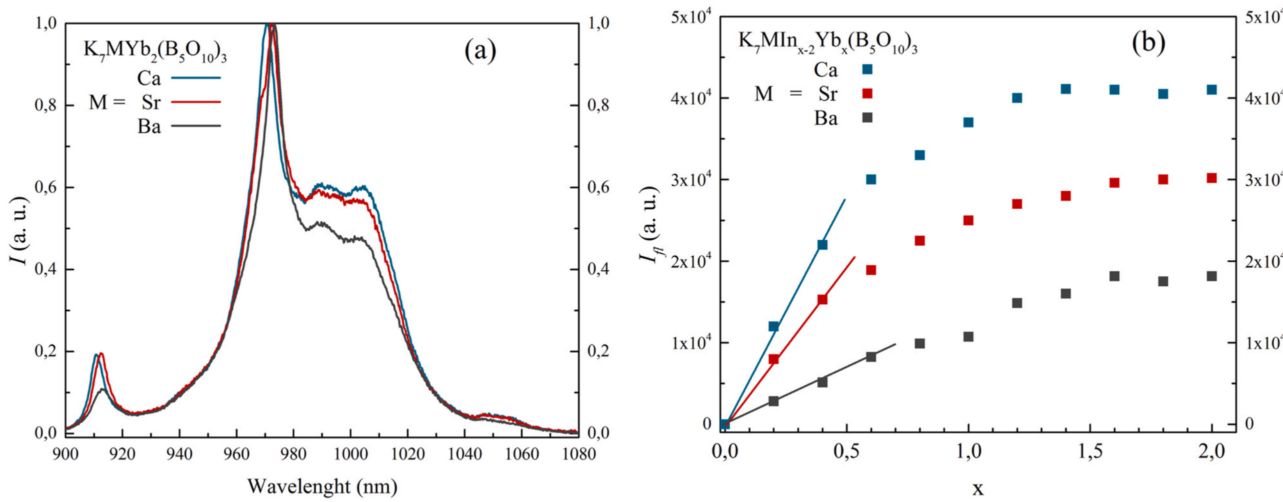

Fig. 6. Spectra (a) and intensity (b) of fluorescence of $K_7MIn_{2-x}Yb_x(B_5O_{10})_3$ (M = Ca, Sr, Ba; x = 0…2) powders.

luminescence in the range of 950–1050 nm and an intense peak at around 790 nm. The luminescence in the near-infrared region is related to $^2F_{5/2}\rightarrow{}^2F_{7/2}$ transitions of Yb^{3+} ions, which is used for the generation of ytterbium lasers operating in a four-level, quasi-four-level, quasi-three-level, or quasi-two-level schemes [32]. Depending on the alkaline earth cation (M), there is an insignificant shift of the spectrum maximum to the long wavelength region with the increase in the atomic mass and, accordingly, the size of the atom, as well as some change in the shape of the spectra. As noted above, according to the data of X-ray phase analysis (Fig. 2), they all have the same structure and crystalized in *R*32 space group; differences in the spectra and luminescence intensities can only be associated with the interaction with the surrounding atoms, and depend on the concentration of the dopant and the nature (size) of the substituent M [33]. It should also be noted that in the samples for the same M and different Yb^{3+} concentrations, there are no changes in the shape and position of the fluorescence maxima.

The dependence of fluorescence intensity on Yb^{3+} concentration is shown in Fig. 6(b). At low concentrations of Yb, the fluorescence intensity increases almost linearly, and then a saturation occurs; this behavior is observed for all M. Fig. 6(b) also shows that, at the same Yb content, the samples with the lighter cation (M = Ca) luminesce better, while the samples with the heaviest cation (M = Ba) luminesce worse. Since there is no clear correlation between the molar mass of the compound and the luminescence intensity [34,35], and for all $K_7MYb_2(B_5O_{10})_3$ there was no concentration quenching achieved, then such a distribution of intensities is most likely associated with the increase in the distance between R atoms.

3.3.2. Second harmonic generation

The syntheses samples are noncentrosymmetric, and therefore are of interest as nonlinear optical materials. Moreover, the use of Yb^{3+}-doped luminescent crystals for SHG is also of interest, since such materials can be considered as active laser medium in SFD lasers [32]. Figs. (7, 8) show the study results of the nonlinear properties of selected materials using Kurtz-Perry powder test for the efficiency of generation of the second harmonic of Nd:YAG laser radiation. SHG intensity versus pump power density for the powder fraction 100–125 µm are shown in Fig. 7, a typical characteristic quadratic dependence of the SHG efficiency on the pump power density is observed.

The SHG intensities for different fractions under pump power density of 50 MW/cm^2 are shown in Fig. 8. As it seen, the efficiency

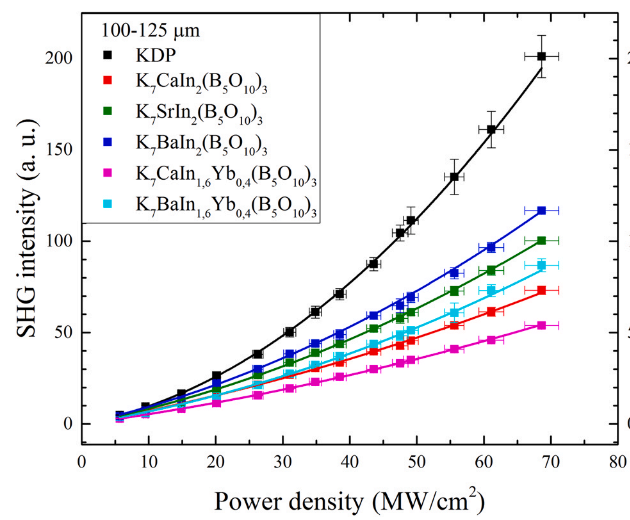

Fig. 7. SHG intensity vs. pump intensity for fraction 100–125 µm.

of SHG for all samples increased with increasing particle size, indicating the implementation of phase-matching synchronism conditions [27].

The three initial samples of $K_7MIn_2(B_5O_{10})_3$ (M = Ca, Sr, Ba) demonstrate a clear dependence of the SHG efficiency on M Fig. 8(a): as the molar mass of the alkaline earth cation increases, the SHG efficiency increases.

To study the effect of partial substitution of indium by ytterbium on the nonlinear properties of crystals, samples with M = Ca and Ba were selected, demonstrating the minimum and maximum SHG efficiencies, respectively. The ratio of ytterbium to indium was chosen to be 1:4; according to Fig. 6(b), when (x = 0.4) there is a linear increase in the luminescence intensity with the ytterbium concentration. It is noticeable that this addition of Yb leads to a drop in the efficiency of nonlinear frequency conversion in crystals by 20–30% (Fig. 8(b), Table 1); this occurs due to the absorption of crystals in the presence of a pump band near the edge of the Yb absorption band. We observed similar results in other borate crystals doped with Yb^{3+} [17]. However, such a drop is not critical, taking into account the multi-pass mode of operation of crystals in intracavity SFD laser systems.

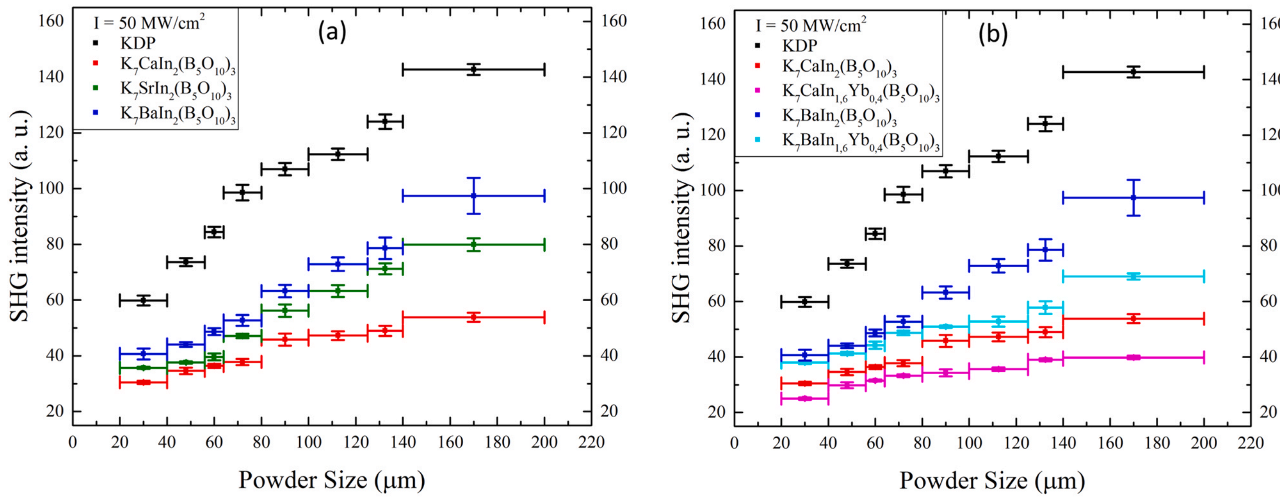

Fig. 8. SHG intensity vs. particle size for pumping power density 50 MW/cm^2.

Table 1
d_{eff} values relative to KDP (I_{pump}=50 MW/cm^2).

Sample	$\frac{d_{eff}}{d_{eff}(KDP)}$
$K_7CaIn_2(B_5O_{10})_3$	0,6670
$K_7SrIn_2(B_5O_{10})_3$	0,7967
$K_7BaIn_2(B_5O_{10})_3$	0,8577
$K_7CaIn_{1.6}Yb_{0.4}(B_5O_{10})_3$	0,5827
$K_7BaIn_{1.6}Yb_{0.4}(B_5O_{10})_3$	0,7289

4. Conclusions

$K_7MIn_{2-x}Yb_x(B_5O_{10})_3$ (M = Ca, Sr, Ba; x = 0…2) compounds were synthesized by the solid state reaction and the crystals were successfully grown by the top seeded solution growth method using the K_2O-B_2O_3-MF_2 flux. According to Rietveld refinement, the crystal structure belongs to the noncentrosymmetric *R*32 space group. Changing the M cation at position allows you to change the distance between R cations within 6.71 Å, 6.72 Å and 7.01 Å for Ca, Sr and Ba, respectively. Thus, as a result of the studies, it was found that studied crystals have intense luminescence and comparable to KDP nonlinear conversion coefficient, which makes them promising for use as an active media in SFD green lasers.

CRediT authorship contribution statement

Ammar Y. Jamous; Investigation, Data curation, Writing- Original draft preparation, Conceptualization, **Valery A. Svetlichnyi;** Formal analysis, Methodology, Investigation, **Artem B. Kuznetsov;** Conceptualization, Investigation, Data curation, Writing- Original draft preparation, **Konstantin A. Kokh;** Validation, Methodology, **Nadezda G. Kononova;** Formal analysis, synthesis, **Ivan.N. Lapin;** Investigation, **Asset Bolatov;** Investigation, **Yerassyl A. Zholdas;** Investigation, and **Alexander E. Kokh;** Methodology, Project administration.

Data availability

No data was used for the research described in the article.

Declaration of Competing Interest

The authors declare that they have no known competing financial interests or personal relationships that could have appeared to influence the work reported in this paper.

Acknowledgment

This work was supported by Russian Science Foundation [№ 22-73-00007], project GF MES RK "Crystallochemical design of the new alkali and rare earth-based borate phosphors" [IRN AP08855427], and state assigned project of IGM SB RAS.

Appendix A. Supporting information

Supplementary data associated with this article can be found in the online version at doi:10.1016/j.jallcom.2022.167912.

References

[1] V. Singh, K.N. Shinde, N. Singh, M.S. Pathak, P.K. Singh, V. Dubey, Green emitting Tb doped $LiBaB_9O_{15}$ phosphors, Optik 156 (2018) 677–683, https://doi.org/10.1016/j.ijleo.2017.11.145
[2] A.B. Kuznetsov, K.A. Kokh, N.G. Kononova, V.S. Shevchenko, V. Kaneva, B. Uralbekov, V.A. Svetlichnyi, A.E. Kokh, Synthesis and growth of new rare earth borates $KCaR(BO_3)_2$ (R= La, Pr and Nd, J. Solid State Chem. 282 (2020), https://doi.org/10.1016/j.jssc.2019.121091
[3] A.B. Kuznetsov, K.A. Kokh, N. Sagatov, P.N. Gavryushkin, M.S. Molokeev, V.A. Svetlichnyi, I.N. Lapin, N.G. Kononova, V.S. Shevchenko, A. Bolatov, B. Uralbekov, A.A. Goreiavcheva, A.E. Kokh, Synthesis and growth of rare earth borates $NaSrR(BO_3)_2$ (R = Ho–Lu, Y, Sc), Inorg. Chem. (2022), https://doi.org/10.1021/acs.inorgchem.2c00596
[4] X. Zhang, X. Chen, C. Zhou, J. Fan, W. Zhou, Q. Pang, L. Zhou, Y. Hu, Synthesis and luminescent property of Ce^{3+} -doped $NaSrY(BO_3)_2$ efficient blue-emitting phosphor as luminescent thermometer, J. Lumin. 251 (2022) 119278, https://doi.org/10.1016/j.jlumin.2022.119278
[5] B. Uralbekov, V. Shevchenko, A. Kuznetsov, A. Kokh, N. Kononova, A. Bolatov, K. Kokh, Novel compounds in the $MMeR(BO_3)_2$ borate family (M = alkali metal, Me = alkaline earth metal, R = rare-earth element): Syntheses, crystal structures and luminescent properties, J. Lumin. 216 (2019), https://doi.org/10.1016/j.jlumin.2019.116712
[6] A. Kuznetsov, A. Kokh, N. Kononova, V. Shevchenko, B. Uralbekov, D. Ezhov, V. Svetlichnyi, A. Goreiavcheva, K. Kokh, New scandium borates $R_xLa_ySc_z(BO_3)_4$ (x+y+z=4, R=Sm, Tb): synthesis, growth, structure and optical properties, Mater. Res. Bull. (2020) 110850, https://doi.org/10.1016/j.materresbull.2020.110850
[7] C. Chen, Y. Wu, R. Li, The anionic group theory of the non-linear optical effect and its applications in the development of new high-quality NLO crystals in the borate series, Int. Rev. Phys. Chem. 8 (1989) 65–91, https://doi.org/10.1080/01442358909353223
[8] R. Li, On the anionic group approximation to the borate nonlinear optical materials, Crystals 7 (2017), https://doi.org/10.3390/cryst7020050

[9] M. Mutailipu, M. Zhang, Z. Yang, S. Pan, Targeting the next generation of deep-ultraviolet nonlinear optical materials: expanding from borates to borate fluorides to fluorooxoborates, Acc. Chem. Res. 52 (2019) 791–801, https://doi.org/10.1021/acs.accounts.8b00649

[10] C. Huang, F. Zhang, S. Pan, Inorganic nonlinear optical materials, reference module in chemistry, Mol. Sci. Chem. Eng. (2022), https://doi.org/10.1016/B978-0-12-823144-9.00081-9

[11] M. Mutailipu, K.R. Poeppelmeier, S. Pan, Borates: a rich source for optical materials, Chem. Rev. 121 (2021) 1130–1202 https://doi.org/10.1021/acs.chemrev.0c00796.

[12] D.A. Hammons, J.M. Eichenholz, Q. Ye, B.H.T. Chai, L. Shah, R.E. Peale, M. Richardson, H. Qiu, Laser action in Yb^{3+}:YCOB (Yb^{3+}:$YCa_4O(BO_3)_3$, Opt. Commun. 156 (1998) 327–330, https://doi.org/10.1016/S0030-4018(98)00460-X

[13] N.I. Leonyuk, Crystal growth of multifunctional borates and related materials, Crystals 9 (2019), https://doi.org/10.3390/cryst9030164

[14] S. Zhao, G. Zhang, J. Yao, Y. Wu, $K_3YB_6O_{12}$: a new nonlinear optical crystal with a short UV cutoff edge, Mater. Res Bull. 47 (2012) 3810–3813, https://doi.org/10.1016/j.materresbull.2012.05.062

[15] S. Zhao, G. Zhang, J. Yao, Y. Wu, $K_6Li_3Sc_2B_{15}O_{30}$: a new nonlinear optical crystal with a short absorption edge, CrystEngComm 14 (2012) 5209–5214, https://doi.org/10.1039/c2ce25304f

[16] A.B. Kuznetsov, D.M. Ezhov, K.A. Kokh, N.G. Kononova, V.S. Shevchenko, S.V. Rashchenko, E.V. Pestryakov, V.A. Svetlichnyi, I.N. Lapin, A.E. Kokh, Flux growth and optical properties of $K_7CaY_2(B_5O_{10})_3$ nonlinear crystal, Mater. Res. Bull. 107 (2018), https://doi.org/10.1016/j.materresbull.2018.07.037

[17] A.B. Kuznetsov, D.M. Ezhov, K.A. Kokh, N.G. Kononova, V.S. Shevchenko, B. Uralbekov, A. Bolatov, V.A. Svetlichnyi, I.N. Lapin, E.A. Simonova, A.E. Kokh, Nonlinear optical crystals $K_7CaR_2(B_5O_{10})_3$ (R = Nd, Yb), growth and properties, J. Cryst. Growth 519 (2019), https://doi.org/10.1016/j.jcrysgro.2019.05.007

[18] M. Mutailipu, Z. Xie, X. Su, M. Zhang, Y. Wang, Z. Yang, M. Janjua, S. Pan, Chemical cosubstitution-oriented design of rare-earth borates as potential ultraviolet nonlinear optical materials, J. Am. Chem. Soc. 139 (2017) 18397–18405, https://doi.org/10.1021/jacs.7b11263

[19] N. Penin, M. Touboul, G. Nowogrocki, Crystal structure of a new lithium indium borate $Li_3InB_2O_6$, Solid State Sci. 3 (2001) 461–468, https://doi.org/10.1016/S1293-2558(00)01144-4

[20] G.M. Cai, J.J. Fan, H.K. Li, Z. Zhao, L.M. Su, Z.P. Jin, Synthesis and relative optical properties of Eu^{3+}/Tb^{3+}-activated $Li_3InB_2O_6$, J. Alloy. Compd. 562 (2013) 182–186, https://doi.org/10.1016/j.jallcom.2013.01.182

[21] S. Divya, S. Das, Eco-friendly $Li_3InB_2O_6$ based red pigments for various IR blocking cool coating applications, Opt. Mater. 109 (2020) 110410, https://doi.org/10.1016/j.optmat.2020.110410

[22] A.K. Subanakov, E. v Kovtunets, S.Z. Choydonov, S.G. Dorzhieva, B.G. Bazarov, New double borate $Rb_3HoB_6O_{12}$: Synthesis and characterization, Kondens. Sredy Mezhfaznye Granit 21 (2019) 278–286, https://doi.org/10.17308/KCMF.2019.21/765

[23] A.K. Subanakov, E.V. Kovtunets, B.G. Bazarov, S.G. Dorzhieva, J.G. Bazarova, New double holmium borates: $Rb_3HoB_6O_{12}$ and $Rb_3Ho_2B_3O_9$, Solid State Sci. 105 (2020), https://doi.org/10.1016/J.SOLIDSTATESCIENCES.2020.106231

[24] K.N. Gorbachenya, V.E. Kisel, A.S. Yasukevich, V.V. Maltsev, N.I. Leonyuk, N.V. Kuleshov, Highly efficient continuous-wave diode-pumped Er, Yb:$GdAl_3(BO_3)_4$ laser, Opt. Lett. 38 (2013) 2446, https://doi.org/10.1364/ol.38.002446

[25] M. Porębski, M. Kowalczyk, L. Gheorghe, M. Greculeasa, A. Broasca, F. Voicu, J. Sotor, Passively mode-locked self-frequency doubling Yb:LGSB laser, in: 2019 Conference on Lasers and Electro-Optics Europe and European Quantum Electronics Conference, Optica Publishing Group, Munich, 2019: p. ca_p_24. http://opg.optica.org/abstract.cfm?URI=CLEO_Europe-2019-ca_p_24.

[26] F. Khaled, P. Loiseau, F. Voicu, A. Achim, S. Hau, C. Gheorghe, G. Croitoru, N. Pavel, L. Gheorghe, G. Aka, Spectroscopic properties and laser performances of Yb:LGSB nonlinear optical crystal, J. Alloy. Compd. 688 (2016) 510–517, https://doi.org/10.1016/j.jallcom.2016.07.048

[27] S.K. Kurtz, T.T. Perry, A Powder Technique for the Evaluation of Nonlinear Optical Materials, 39 (1968) 3798–3813. https://doi.org/10.1063/1.1656857.

[28] R.L. Sutherland, D.G. McLean, S. Kirkpatrick, Handbook of Nonlinear Optics, Marcel Dekker, New York, 2003.

[29] W.J. Alford, A. v Smith, Wavelength variation of the second-order nonlinear coefficients of $KNbO_3$, $KTiOPO_4$, $KTiOAsO_4$, $LiNbO_3$, $LiIO_3$, β-BaB_2O_4, KH_2PO_4, and LiB_3O_5 crystals: a test of Miller wavelength scaling, J. Opt. Soc. Am. B 18 (2001) 524–533, https://doi.org/10.1364/JOSAB.18.000524

[30] F. Zernike, J.E. Midwinter, Applied Nonlinear Optics, John Wiley, New York, 1973.

[31] R.D. Shannon, Revised effective ionic-radii and systematic studies of interatomic distances in halides and chalcogenides, Acta Crystallogr. Sect. A 32 (1976) 751–767. https://doi.org/Doi 10.1107/S0567739476001551.

[32] D. Lu, H. Yu, H. Zhang, J. Wang, Q. Fang, X. Yu, X. Han, Power scaling of the self-frequency-doubled quasi-two-level Yb:YCOB laser with a 30% slope efficiency, Opt. Lett. 44 (21) (2019) 5157–5160, https://doi.org/10.1364/OL.44.005157

[33] R.J. Wiglusz, G. Boulon, Y. Guyot, M. Guzik, D. Hreniak, W. Strek, Structural and spectroscopic properties of Yb^{3+}-doped $MgAl_2O_4$ nanocrystalline spinel, Dalton Trans. 43 (2014) 7752–7759, https://doi.org/10.1039/C3DT53644K

[34] Y.Q. Li, G. de With, H.T. Hintzen, Luminescence properties of Ce^{3+}-activated alkaline earth silicon nitride $M_2Si_5N_8$ (M=Ca, Sr, Ba) materials, J. Lumin. 116 (2006) 107–116, https://doi.org/10.1016/J.JLUMIN.2005.03.014

[35] S. Lizzo, A. Meijerink, G. Blasse, Luminescence of divalent ytterbium in alkaline earth sulphates, J. Lumin. 59 (1994) 185–194, https://doi.org/10.1016/0022-2313(94)90040-X